npj | climate and atmospheric science

Article

Published in partnership with CECCR at King Abdulaziz University

https://doi.org/10.1038/s41612-024-00863-3

Improve the projection of East China summer precipitation with emergent constraints

Huanhuan Zhu[1,2], Zhihong Jiang[2] ✉, Laurent Li[3], Wei Li[2] & Sheng Jiang[2]

Under global warming, summer precipitation over East China was projected to increase by current state-of-the-art climate models, but a large inter-model spread exists. Here we try to reduce the projection uncertainty by imposing constraints. Our procedure consists of first decomposing the projected future precipitation into inter-model principal components. The two leading modes (region-wide uniform monopole and north-south dipole, accounting for 55% of variability), by emergent constraints, are then linked to the simulation of historical precipitation in the northwest Pacific and the tropical Pacific (constraining areas). This allows us to reduce the uncertainties by 23% and obtain a smaller increase of projected precipitation in East China, relative to previous multi-model ensemble projections. Quasi-uniform increases, although weak, are obtained for the first mode, while the second mode shows a contrast pattern with a decrease in the south and an increase in the north, which both contribute to the spatial structure of constrainted projection. It is also shown that the emergent relations of both modes are physically consistent, with an enhancement of future zonal land-sea thermal contrast and a La Niña-like pattern, respectively. The use of emergent constraints inspires more confidence in the future regional precipitation projection and helps policymakers and stakeholders adjust their management policies.

East Asian summer monsoon (EASM) is a major component of the global climate system and plays an important role in determining the East Asian climate and its variation[1]. The summer monsoon provides the majority of the annual precipitation of the region. Due to the unique geographical location and topography in East Asia, the summer monsoon shows complex behaviors with multi-scale spatio-temporal variability[2–6], which makes a challenging issue its reliable projection under global warming.

Reported studies based on climate models generally show an increase of the East Asian summer monsoon precipitation (including East China summer precipitation, ECSP) under warmer climate, partly explained by increased atmospheric water vapor content[7,8], or as a result of enhanced East Asian summer monsoon circulation under global warming[7,9]. But there is a remarkable inter-model spread on both intensity and spatial pattern among models[10–15]. Zhu et al. showed that the annual total precipitation will increase by 5.4% and 11.2%, relative to 1995-2014, over China under 1.5 °C and 2 °C global warming levels, but with significant regional differences for the projection reliability[15]. The regional average signal-to-noise ratio of annual and seasonal precipitation changes under 1.5°C global warming is estimated to be less than 0.1[16], indicating the existence of big uncertainty. The reduction of uncertainty of future projection of the ECSP needs thus a great effort of the scientific community.

Model biases in simulating the observed climate are a major source of uncertainty and can impede our confidence in regional climate projections. This consideration leads us naturally to the intuitive idea that we might search for a relationship between a current modeled but observable variable and a projected variable in the future climate. At the same time, the diversity of climate models allows us to deduce this link from inter-model relations. Such a procedure is generally known as the technique of emergent constraint[17–20]. It needs however to be noted that this inter-model relationship should be explainable with physical principles for it to be confident.

In the literature, we can see that many factors, such as the SST over cold-tongue and marine stratocumulus regions[21], the convection over the western Pacific[12], and the interhemispheric thermal contrast[22] have been used to constrain the projection of summer precipitation over the East Asian

[1]Key Laboratory of Ecosystem Carbon Source and Sink, China Meteorological Administration, Wuxi University, Wuxi, China. [2]Key Laboratory of Meteorological Disaster of Ministry of Education, Collaborative Innovation Center on Forecast and Evaluation of Meteorological Disaster, Nanjing University of Information Science and Technology, Nanjing, China. [3]Laboratoire de Météorologie Dynamique, CNRS, Sorbonne Université, Ecole Normale Supérieure, Ecole Polytechnique, Paris, France. ✉e-mail: zhjiang@nuist.edu.cn

and Afro-Asian monsoon regions. But it is still unclear what is the right and efficient way to find the just constraining factors or variables with the emergent constraint technique. The lack of a systematic procedure with a normalized implementation is actually an obstacle for the emergent constraint method to be more exploitable by the scientific community. These two points constitute our main motivation to perform the present work. For the practical application, the case of East China summer precipitation will be used.

The East Asian climate system is of high complexity, it is a challenging issue to identify the key physical processes affecting the projection of precipitation. Meanwhile, the bias of model simulation is also large, and makes it difficult to diagnose these key physical processes from model data. Based on coupled models participating in phase 6 of the Coupled Model Intercomparison Project (CMIP6), this study aims to answer the following two questions: 1) What is the source of the inter-model spread of ECSP projection under global warming? 2) How to constrain the projected change of ECSP based on emergent constraints?

Here we construct a general framework of the emergent constraint technique for ECSP projection. The future precipitation projected by the ensemble of CMIP6 models was first decomposed into inter-model principal components. The leading modes were then linked to the simulation of the present-day potential constraining variables (rainfall in the tropical Pacific). The current-to-future emergent relationship deduced from inter-model variability helps to reduce the uncertainty, with the constraining effect of the observed predictor. It shows a smaller increase of projected precipitation in East China in a warmer future with about 23% of the projection uncertainty reduced, relative to previous multi-model ensemble projections.

Results

Leading modes of inter-model spread in the ECSP projection

CMIP6 models project a general increase in East China summer precipitation (ECSP) under the high-emission scenario, Shared Socioeconomic Pathways (SSP) 5-8.5 (2070-2099), relative to 1985-2014. Larger increases of ECSP occur over north China for the multi-model ensemble mean (MME). But individual models show some diversity, and even a few models project a decrease for ECSP, such as MIROC-ES2L and NorESM2-LM (Supplementary Fig. S1). This indicates that there is a large inter-model spread in the projected ECSP.

To reveal the sources of model spread, we conduct an inter-model empirical orthogonal function (EOF) analysis on the projected changes of ECSP (Fig. 1, see Methods). The first two leading principal components (*PC1* and *PC2*) account for 55% of the total inter-model variance. The leading pattern EOF1 shows a monopole structure across East China, with large loading in the north subregion (Fig. 1a). It explains 39.3% of the inter-model variance. EOF2 shows a dipole structure, with the transition line at about 35°N (Fig. 1c). It explains 15.7% of the inter-model variance. Because these two leading modes include an important part of the total variability, it would be possible to reduce the uncertainty of ECSP projections if their *PCs* can be observationally constrained.

Historical constraining variables and their spatial patterns

To appropriately select constraining indices, we regressed model simulated historical mean state (1985-2014) of potential constraining variables (SST, precipitation, geopotential height and vertical velocity at 500 hPa, zonal and meridional wind at 850 hPa) in boreal summer onto the normalized *PC* across models. The basic principle of selecting the right predictor on the

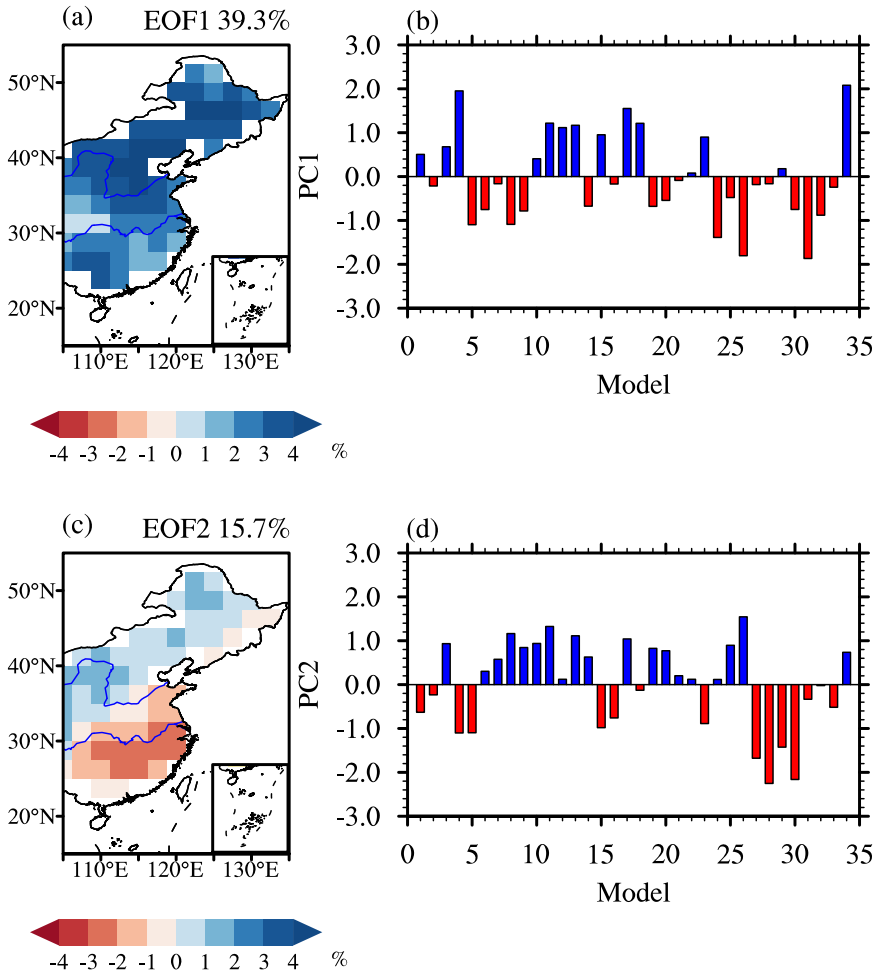

Fig. 1 | Projected leading inter-model spreading modes and related normalized principal components. The two leading modes (EOF1 and EOF2, **a** and **c**) derived from inter-model empirical orthogonal function (EOF) analysis on the projected changes of ECSP. Value on the top-right corner is the explained inter-model variance. The corresponding first and second normalized principal components (*PC1* and *PC2*, **b** and **d**). Each number (horizontal coordinate) represents an individual model listed in Table S1.

right space is that the constraining areas for the predictor should have a good correlation with the predictand (here *PCs*) and a clear physical meaning. We find that the first mode is linked to a positive precipitation (ascent) anomaly in the northwest Pacific (8°N-25°N, 120°E-180°E), stretching eastwards from the Philippine Sea to the central Pacific (Fig. 2a and Supplementary Fig. S2a). This mode indicates that if a model has wet bias (ascent anomaly) in the northwest Pacific region in the historical simulation, its projected future ECSP tends to be wetter as shown in the EOF1 (Fig. 1a). The first mode is also linked to a positive zonal wind anomaly over the western Pacific and South China Sea (0°N-15°N, 90°E-180°E), stretching eastwards from the eastern Indian Ocean to the central Pacific (Supplementary Fig. S3a).

The second mode is associated with precipitation (vertical velocity) anomalies over the low-latitude tropical Pacific (8°S-25°N, 120°E-90°W), where the regression pattern signs are reversed at 5°N (Fig. 2b and Supplementary Fig. S2b). This mode indicates that if a model has wet bias (ascent anomaly) in the South equatorial Pacific and dry bias (descent anomaly) in the North equatorial Pacific in the historical simulation, its projected future ECSP tends to be heavier in the north and lighter in the south, as shown in the EOF2 (Fig. 1b).

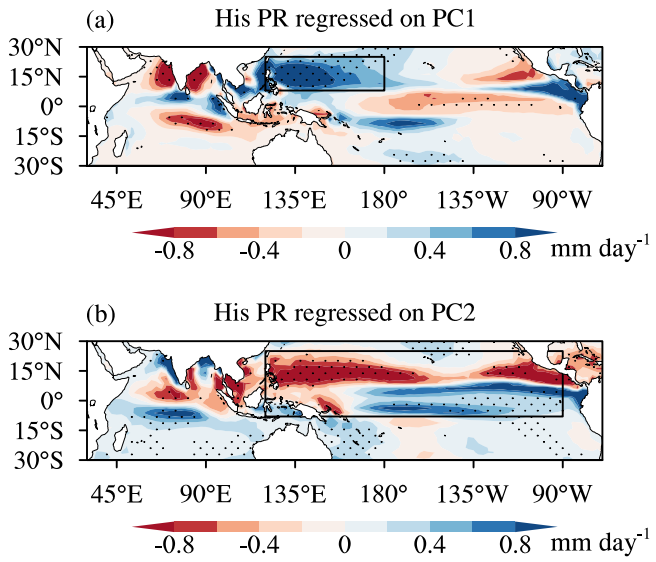

Fig. 2 | Historical model spread patterns of precipitation (PR) associated with the principal components. From top to bottom are the first principal component (*PC1*, **a**) and the second principal component (*PC2*, **b**). Black boxes in **a** and **b** are used to define constraining indices to constrain the *PCs*. Dotted regions are statistically significant at the 5% level under Student t-test.

Projection of ECSP under constraints

The relationship between PR patterns and the leading modes of inter-model spread established above exerts constraints on the ECSP projection, using relatively reliable precipitation observations. We firstly produce two constraining indices (*CIs*) to measure the model's fidelity in simulating the observed climate in the historical period by projecting the mean-state precipitation onto the two precipitation modes associated with the inter-model leading *PCs* shown in Fig. 1a and c (see Methods). *CI1* is for the northwest Pacific (black box in Fig. 2a) and *CI2* for the low-latitude tropical Pacific (black box in Fig. 2b). These two indices are also calculated for the two observations to serve as the reference to evaluate models. *CI1* is larger than observation in more than 90% of the models, which means that simulated precipitation in most models is above the observation over the northwest Pacific. *CI2* is smaller than observation in about 65% of the models, indicating that the majority of models simulate less precipitation than observed in the South equatorial Pacific and more precipitation in the North equatorial Pacific.

A linear regression across models between the current climate (PR pattern indices, X) and projected changes (*PCs*, Y) is then performed: $Y = \bar{Y} + k(X - \bar{X})$, where k is the regression coefficient, and $\bar{X}$ and $\bar{Y}$ are the MME (see Methods). The PR pattern indices can well explain the leading modes of inter-model spread in projected ECSP, as evinced by the significant correlation coefficient with the *PC1* ($r = 0.65$, $p < 0.01$; Fig. 3a) and the *PC2* ($r = 0.67$, $p < 0.01$; Fig. 3b). Based on the relationship and observational PR pattern indices, we can estimate the *PCs* and reduce their variances. For *PC1* and *PC2*, the reduced variances are about 40% and 44%, respectively, mainly determined by the high correlation coefficients with *CI1* and *CI2* (Fig. 3). Considering the fact that the explained variances by *PC1* and *PC2* are 39.3% and 15.7%, respectively (Fig. 1), we can deduce that the total variance reduction by the emergent constraints is about 23% (40% × 39% + 44% × 16%). The constrained value of *PC1* is −0.68 ± 0.77 and *PC2* is 0.31 ± 0.76 (mean value with ±1σ; Fig. 4).

We can now further reconstruct the spatial patterns of the ECSP projection with the optimal *PCs* and their spatial patterns. The constrained projection shows an increase of summer precipitation across East China at the end of the 21st century (2070-2099, relative to 1985-2014, Fig. 5a), with the areal-mean increase exceeding 14.8%. The largest increase is in the northern subregion, the smallest over the Yangtze River basin. The constrained projection shows a prominent decrease of the ECSP (Fig. 5c), compared to the original MME without the emergent constraints (Fig. 5b). The largest decrease is in the central and north areas, exceeding 3%. A further assessment on the contribution of each mode reveals that the

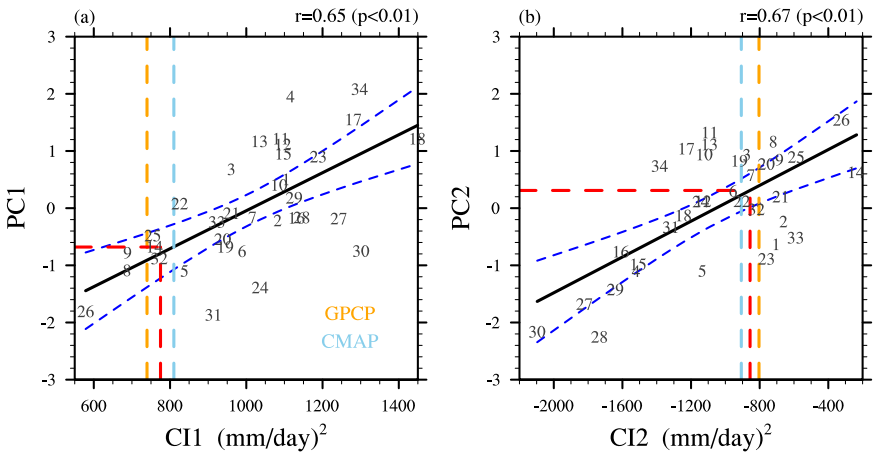

Fig. 3 | Inter-model emergent relationship between the summer precipitation projection (represented by *PC1* and *PC2*) in East China and the historical precipitation patterns in the tropical Pacific (represented by *CI1* and *CI2*). *CI1* in **a** and *CI2* in (**b**) measure how the precipitation patterns in black boxes in Fig. 2 are simulated in the historical simulation. Correlation coefficients (statistically significant at the 1% level with a Student t-test) are displayed on the top right corner. Bold black fitting line is obtained by the least square method. Blue dashed curves denote the 95% confidence range of the linear regression. *CI1* and *CI2* indices from two observational precipitation datasets (GPCP and CMAP; vertical dashed lines) are used to constrain the values of *PCs*. The mean of the two observational results yields the optimal constraint (red dashed lines). Each number represents an individual model listed in Table S1.

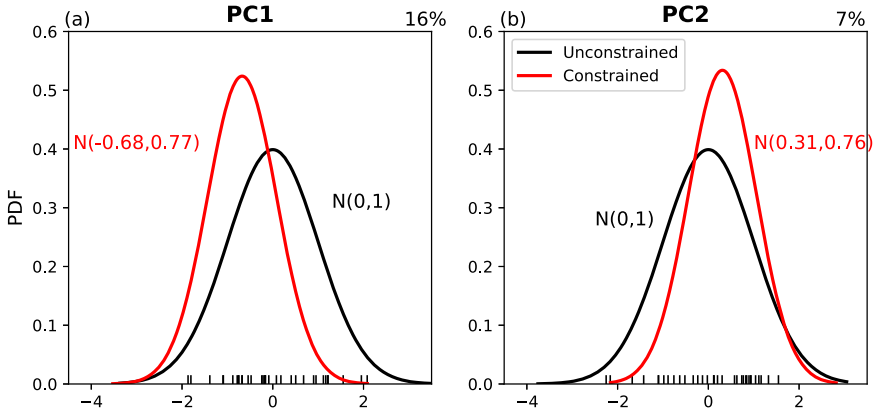

Fig. 4 | Probability density function of original and constrained principal components. Probability density functions of the first and second principal components (*PC1* in **a** and *PC2* in **b**) are generated with the Gaussian assumption. The figures on the right corner are the percentage of variance reduced by the emergent constraint. The mean and the standard deviation of the Gaussian function are shown in the parentheses after the letter N. Short vertical lines denote the original *PC* values of each model.

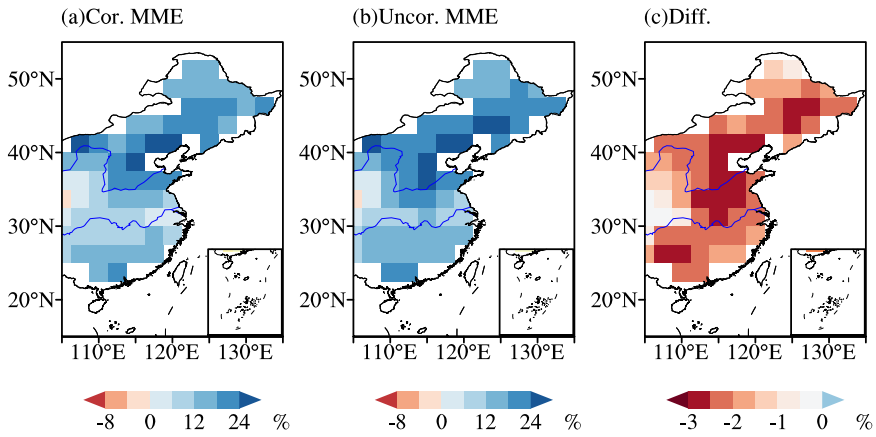

Fig. 5 | Corrected projections and differences from the uncorrected. Corrected (**a**) and uncorrected (**b**) East China summer precipitation projection in the multi-model ensemble mean (MME) based on the best-estimated principal components (see details in "Methods"). The difference (**c**) between corrected and uncorrected results, which is reconstructed by the two constrained leading uncertainty modes (Supplementary Fig. S4).

projected ECSP change, by the first mode, shows a uniform reduction (relative to the MME), with a significant decrease in the north of the region (Supplementary Fig. S4a). By the second mode, the projected ECSP increase is larger than the MME in the north, and smaller in the south (Supplementary Fig. S4b). The smaller amplitude of rainfall increase for the constrained projection in East China is mainly contributed by the constraining effect through EOF1.

Robustness of the emergent relation

A particularity of the emergent constraint procedure is that the statistical relationship (a linear regression) between the predictor and the predictand is established through inter-model variability. For our purpose, there is a linkage between the future projection of precipitation in East China and the distribution of precipitation over the tropical oceans in the historical period. It is important for us to ensure that such a relationship is a robust one. In the absence of an easily-explained mechanism, we can nevertheless gain some confidence by examining the physical coherence among different geophysical variables going through the emergent constraint procedure.

Parallel to Panels a and c (Fig. 1) which are the projection of rainfall anomalies onto the inter-model principal components, as shown in Panels b and d in Fig. 1, we can apply the same operation of regression to the projected changes of any geophysical variables by regressing them onto the *PCs*.

For the surface temperature (Fig. 6), we find a uniform warming pattern over East Asia related to *PC1* but with evident regional disparity, exhibiting land-sea thermal contrast, with obviously strong warming over south of 35°N in eastern China land area. This means that the zonal (east-west) sea-land thermal contrast in East Asia increases, which could enhance the East Asian summer monsoon circulation, and lead to rainfall increase under global warming[7]. The regression patterns of precipitation changes onto *PC1* show a weak (strong) increase in the South China Sea (East China). There is an anomalous anticyclonic pattern of lower-level circulation changes over East Asia, with easterly winds in the northwest Pacific (Fig. 6b). East China is located on the northwest flank of the anticyclone, and the local southerly winds increase the water vapor transport from the South China Sea and the northwest Pacific, leading to a strong increase in precipitation over East China. There exist obvious ascents over East China, with stronger ascents around 30°N-40°N, associated with significantly stronger precipitation (Supplementary Fig. S5). The 850hPa circulation presents southerly winds over East China, indicating abundant water vapor.

The above analysis of the emergent relationship clearly indicates that if a model simulates more historical precipitation in the northwestern Pacific, its projected ECSP increase is amplified. Such a conclusion is due to the enhancement of future east-west sea-land thermal contrast and to the presence of an anomalous low-level anticyclone over East Asia, leading to stronger ascents in eastern China. The inter-model spreading mode of future surface temperature change associated with *PC1* shows a structure similar to the global warming pattern (larger warming over land than over sea, and at higher latitudes than at lower latitudes), suggesting that *PC1* is partly related to model spread in global mean surface temperature (GMST) projection (Supplementary Fig. S6) or climate sensitivity. A model simulating more historical precipitation in the northwestern Pacific will project larger GMST increase, which influences the future east-west sea-land thermal contrast between the East China land area and the subtropical Northwest Pacific (Fig. 6). Larger future east-west sea-land thermal contrast means stronger East Asian summer monsoon, and leads to stronger precipitation increase (*PC1*) in eastern China. Although now we cannot formally prove the significant relationship between the present-day precipitation over the western Pacific and climate sensitivity, our hypothesis

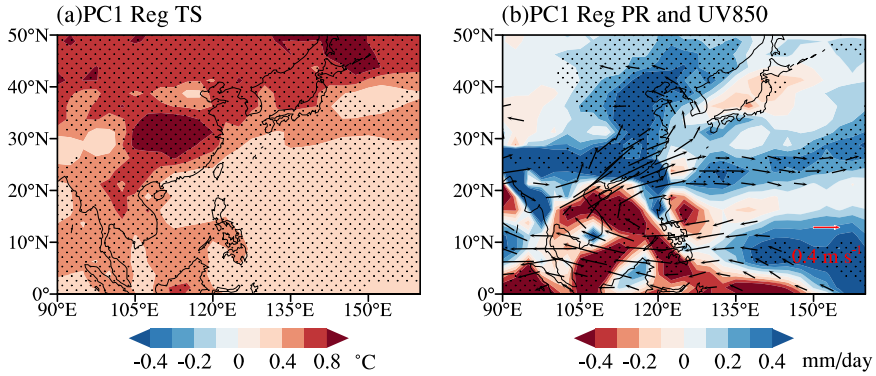

Fig. 6 | Inter-model regressions of future changes onto the first principal component (*PC1*). Changes in summer-mean (**a**) surface temperature, (**b**) precipitation (shadings), and 850 hPa winds (vectors). Dotted shadings are statistically significant at the 5% level under the Student t-test.

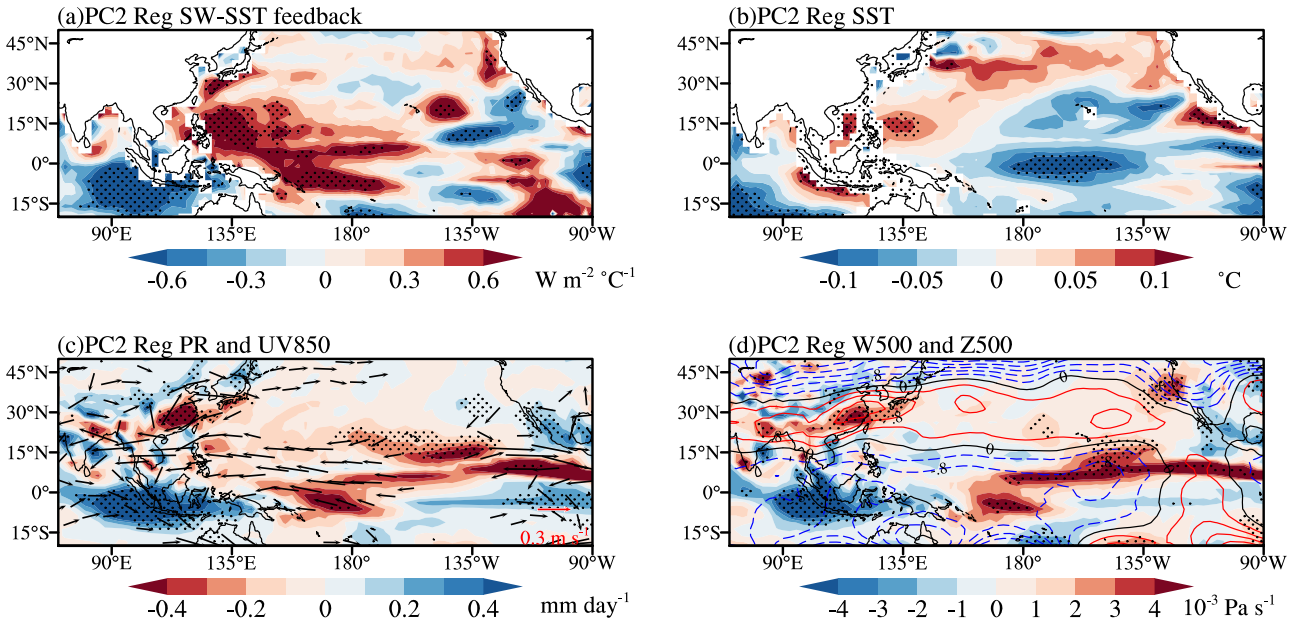

Fig. 7 | Physical processes related to model uncertainties in projection of the second mode. Inter-model regressions of (**a**) SW-SST feedback in the historical experiment and future changes in summer-mean (**b**) sea surface temperature, (**c**) precipitation (shadings) and 850 hPa winds (vectors), (**d**) 500 hPa vertical velocity (shadings) and geopotential height (contours) onto the second principal component (*PC2*). Dotted shadings are statistically significant at the 10% level under the Student *t*-test.

seems supported by the rich literature discussing the pattern effect of climate sensitivity[23–25].

For the second leading mode, we find that the negative shortwave radiation-SST (SW-SST) feedback related to convective clouds in tropical regions plays an important role in linking the historical tropical Pacific precipitation and future local SST warming pattern, which could influence the East China summer precipitation changes. Following Chen et al. [21], the SW-SST feedback is defined as the change of surface downwelling shortwave cloud radiation (R_{SWC}) for per degree SST: SW-SST feedback = δR_{SWC} / δSST. R_{SWC} is calculated by the radiation flux of all-sky minus that of clear-sky. In the western Pacific, the suppressed precipitation leads to decreased convective cloud and impairs the negative SW-SST feedback (Fig. 7a). Accordingly, the impaired negative SW-SST feedback increases the incident shortwave and amplifies the warming in the western Pacific (Fig. 7b). In contrast, the excessive precipitation in the Central equatorial Pacific triggers the strong negative SW-SST feedback and generates a reduced SST warming therein in the future. So, we can see the positive (negative) SST anomalies in the western Pacific and East equatorial Indian Ocean (Central equatorial Pacific) are related to *PC2*. The spatial pattern of SST presents the inverse phase of the Tropical Pacific-Indian Ocean associated mode[26], corresponding to the typical central Pacific La Niña. This indicates that if a model simulates more precipitation in tropical regions in the current climate, it will project a weaker local SST warming. This is because the negative SW-SST feedback related to convective clouds in tropical regions is an important mechanism to damp SST anomalies[12,21,27].

The regression patterns of precipitation changes onto *PC2* show a weak (strong) increase in the equatorial Pacific of 160°E-170°W and south East China (Maritime Continent and equatorial East Indian Ocean) regions. There is an anomalous anticyclonic pattern of low-level circulation changes over East China to Japan, easterly winds in the equatorial western Pacific, and northeastward winds from the Indian Ocean and the Arabian Sea, which leads abundant (less) water vapor to North (South) China (Fig. 7c). The 500 hPa vertical velocity shows a strong descent (ascent) in the southern part of East China and the equatorial West Pacific (northern part of East China and the equatorial eastern Indian Ocean regions). The 500 hPa geopotential height presents the inverse phase of the East Asia-Pacific (EAP) teleconnection type, showing a tripolar pattern of "minus-plus-minus" from south to

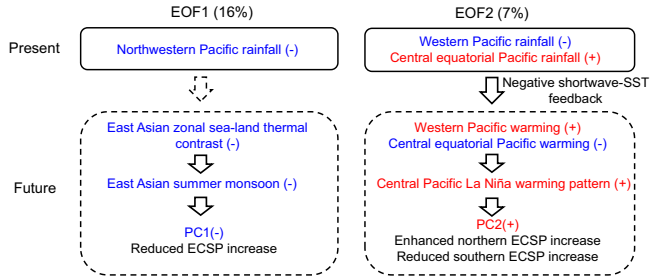

Fig. 8 | A summary of the physical processes connecting the present-day rainfall in the tropical Pacific and the projected East China summer precipitation (ECSP) changes. Solid boxes denote processes in the historical period and dashed boxes for future projection. Red: processes that are stronger (+) in observation than historical simulation in multi-model ensemble mean (MME) or enhanced (+) in future changes than the original projection in MME. Blue: opposite to the red. Percentages on the top are reduced variances after constrained by observational rainfall for the two leading inter-model empirical orthogonal function (EOF) modes (EOF1 and EOF2) of the projected ECSP changes. The constrained results for the first mode favor a reduced ECSP increase, and for the second mode favor a reduced (enhanced) precipitation increase in south (north) East China, represented by a negative value of the first principal component (*PC1*) and a positive value of the second principal component (*PC2*).

north in East Asia (Fig. 7d). There exist obvious ascents (descents) over northern (southern) East China, associated with dipole precipitation changes. The 850 hPa circulation presents a weak northerly wind over southern East China, and the 200 hPa jet stream shows a strong northward shift, which is not conducive to the southward motion of cold air from the north. The geopotential height also shows a significantly positive anomaly over south of 35°N in East China, which corresponds to the local anticyclonic anomaly and descent (Supplementary Fig. S7). The corresponding circulation patterns make the precipitation increase more (relative to MME) in the north and less in the south. Many studies[28,29] have shown that such a circulation response is closely related to the SST pattern in the tropical Pacific.

The above analysis shows that if a model simulates less (more) current precipitation in the north of the equatorial Pacific (central-eastern equatorial Pacific) than the MME does, its projected future ECSP increase tends to be larger (smaller) in the north (south) of East China, which is closely related to a typical central Pacific La Niña warming pattern through the shortwave-SST negative feedback. If a model simulates more precipitation in the current climate, it will maintain (even enhance) the shortwave-SST negative feedback both on historical and future periods, and project a weaker local SST warming and precipitation increase (Fig. 7 and Supplementary Fig. S8). Actually, atmospheric convection in the equatorial Pacific region, sensitive and responsive to surface warming, can suppress local surface warming by modulating the surface net shortwave flux and introducing negative feedback[12]. Recently, some scholars also believe that East China precipitation increasing more (less) in the north (south) may be related to an increase in the east-west SST gradient over the Pacific, which results from the stronger SST warming in the western Pacific than in the central Pacific[30].

Key processes backing the emergent constraints on the two basic modes of ECSP projection are summarized in Fig. 8. It should be noted that the panel related to EOF1 in Fig. 8 starts the process description by a decrease of rainfall over the Northwestern Pacific (not an increase over the same oceanic basin, as in Fig. 3a which might have a reversed sign if its *PC* is reversed) to mimic the fact that observed rainfall in that region is smaller than the simulated rainfall in the multi-model ensemble mean. There is a reduction of about 23% for the CMIP6 inter-model variance, a consequence of the emergent constraints. Through correcting the wet biases in the northwest Pacific and dry biases in the equatorial Pacific, we conclude that the ECSP increase will weaken (relative to MME) in a future warming climate. The constrained projection will indicate a monopole increase of the ECSP changes, with largest increase in the north (Fig. 5).

Discussion and outlook

This study aims to reduce the uncertainty of East China summer precipitation projection by the implementation of emergent constraints. In this section, we summarize several robust and important findings and conclusions of regional precipitation projections, and discuss the limitations and the future research directions of this work.

Our emergent constraint on the projection of ECSP is based on SSP5-8.5 scenario. The future precipitation projected by the ensemble of CMIP6 models under the SSP5-8.5 high emission scenario was firstly decomposed into inter-model principal components. The two leading modes were then linked to the simulation of the present-day rainfall in the tropical Pacific, which can serve as constraining factors. Then, the current-to-future emergent relationship deduced from inter-model variability helps to reduce the uncertainty, with the constraining effect of the observed precipitation in the tropical Pacific (the constraining area). Finally, the plausible mechanism of the emergent relation was analyzed.

We found that the two leading modes of inter-model variability account for 55% of the total variance (inter-model spread) in projecting ECSP by the end of the 21st century. The first mode shows a monopole spatial structure across East China, with larger loadings in the north. The second mode shows a dipole structure, with the demarcation at 35°N. The two leading modes are related to the simulation of historical precipitation in the northwest Pacific and tropical Pacific, respectively. Based on the current-to-future inter-model emergent relationship and on the observed precipitation in the constraining areas, the constrained projections reduce the uncertainties by 23% and indicate a monopole increase of the ECSP changes, with the largest increase in the north. But it is lower than the original multi-model ensemble mean, especially over the north subregion.

We extended our analysis to SSP2-4.5 scenario and got similar conclusions (Supplementary Figs. S9–11). In addition, to examine the robustness of the emergent constraint, we also checked the inter-model emergent relationship between *CIs* and *PCs* by using different subsets of models (Supplementary Fig. S12 and S13) and different periods (Supplementary Fig. S14), and we came to similar conclusions. The independence of the results on the model ensembles, periods, and future emission scenarios confirms the robustness of the conclusions.

Our corrections reduce the uncertainty in ECSP projection by removing the influence of the low-latitude Pacific precipitation biases, but our method does not rule out the effects of other model biases. The cold-tongue bias in the tropical eastern Pacific and a cold bias in marine stratocumulus cloud regions have been proven to be closely related to the western North Pacific Subtropical High projection[21]. Projections of a wetter winter for the US Southwest and a drier winter for the Mediterranean basin under global warming are significantly influenced by a common model bias featuring a double Intertropical Convergence Zone[31]. The potential impact of these model biases on ECSP projection needs further investigation.

Our results suggest that improving the simulation of tropical Pacific convection and rainfall is an important step to reach more reliable projection of summer precipitation over East China. This will urge model development for bias reduction in the tropical Pacific precipitation. It is also possible that these targeted development activities would lead to a reduction of model spreading, which could eventually lead to the disappearance of the emergent relationships.

More confidence in the future precipitation projection in East China based on emergent constraints will be likely to improve the understanding of the impacts for a warmer climate and help policymakers and stakeholders adjust future management policies. Besides, the employed emergent

constraint technique can be helpful to other parts of the world in tackling the model bias to develop reliable regional climate change projections.

Previous studies have also employed different constraining methods on ECSP projection[12,22,32]. For instance, Zhou et al.[32] introduced a bias-correction method to correct the multi-model projection of changes in East Asian summer monsoon rainfall and found a pronounced increase zone in southern China and an increase belt from northern China to northeastern China. Results from Chen et al.[22] revealed that the projection with model raw output overestimates the increase of precipitation in the East Asian summer monsoon regions, which is consistent with our findings.

It is interesting to note that most studies employing the procedure of emergent constraints generally focus on precipitation projection at global[33,34] or hemispheric scales[22,35,36]. That is, they generally quantified a single value of areal mean, and did not consider the pattern or spatial structure of precipitation. In our work, however, the spatial structure of precipitation is considered in the constrained projection.

Two datasets of precipitation observation were used in this work, from different sources (GPCP and CMAP), showing apparent discrepancies in the tropical Pacific (Fig. 3). It is clear that future improved observations can bring further positive contributions for this issue. Observed data reflect one realization of many possibilities of a complex climate system, and there exist uncertainties for the observationally constrained projections. Observations require further quality control or using multiple observations so that they can work better for observational constraints[18,21]. Like the real world, climate models have internal variability. Because of the finite length of the simulation or observed climate record, internal variability can have a significant impact on the estimation of the predictor. One possibility is to use very long model control simulations to estimate the size of internal variability if it is believed to be independent of forcing[37]. Using large ensemble experiments to quantify the effect of internal variability is another way[38].

In terms of future evolution of the emergent constraint technique, we may suggest several directions to pursue. Most works on emergent constraints used just two scalar variables, a predictor X, and a response or predictand Y, related linearly. This could be extended to two or more predictors or predictands. But we don't know yet whether these emergent constraints can or cannot be combined, and how to perform such a combination[18,39]. It is also important to acknowledge that only the signal in the tropics is considered in this work, mid-latitude and even high-latitude climate properties can also affect the East Asian summer monsoon, and provide potential constraints to its variation.

Methods

Model data and observation

Historical simulation and future projection under SSP5-8.5 scenario from 34 (maximum available number) CMIP6 models are used (Table S1) in this study. The historical experiments start from the pre-industrial experiment and are forced by observed natural and anthropogenic conditions during 1850-2014. The SSP5-8.5 experiments take the way of Fossil-Fueled Development and its radiative forcing reaches 8.5 W m^{-2} in 2100[40]. Because a few CMIP6 models provided only a single realization for the SSP5-8.5 projection, we decided to use, for all models, their first realization member. To check the independence of results on the default emission scenario, we also use the SSP2-4.5 scenario in our investigation. To represent future projection of the ECSP, we focus on the changes of summer total amount of precipitation during June, July, and August over East China between 2070-2099 and 1985–2014. Main climate variables used in our work are monthly surface temperature (Ts, i.e., SST in the ocean), precipitation (Pr), horizontal wind (U and V), vertical velocity (ω), geopotential height (Z), and surface downwelling shortwave radiation.

In terms of observation, monthly precipitation from Global Precipitation Climatology Project (GPCP) version 2.3 dataset[41] and the Climate Prediction Center (CPC) Merged Analysis of Precipitation (CMAP) dataset[42] are adopted. The same period of 1985-2014 as the model baseline is used to calculate the mean state in the observation. All data are re-gridded to a common 2.5° × 2.5° mesh using bilinear interpolation.

Inter-model empirical orthogonal function analysis

The leading modes of inter-model spread in the ECSP projection in the domain (15-55°N, 105-135°E) are analyzed with a typical EOF method, applied to the spatial dimension:

$$P(m,n) \cong \sum_{i=1}^{I}\left\{PC_i(m) \times EOF_i(n)\right\} \quad (1)$$

where $P(m,n)$ is the projected changes of ECSP (expressed as a deviation from the multi-model ensemble mean, MME) for the model numbered m among the M models in total (34 here) and the grid numbered n in the space N (target area, or area to be constrained, here covering East China). $i(\in I)$ represents the number of decomposed modes (two leading modes here). Here, each PC_i is normalized. The eigenvalue in each mode is merged into the corresponding EOF. The inter-model EOF decomposition has been successfully used in investigating the East Asia monsoon[12,21,22].

Definition of constraining indices

To appropriately select predictors, we consider the simulated historical mean state (1985-2014) of a potential constraining variable, noted as $H(m,l)$ for model m and space grid $l \in L$. We remind that the space L represented by l can be different from the space $n \in N$ in $P(m,n)$. The former (l) is the constraining area, while the latter (n) is the area to be constrained. The generic variable H can be SST, precipitation, geopotential height and vertical velocity at 500 hPa, zonal and meridional wind at 850 hPa or any other geophysical variables with potential constraining effects on P. If we now project $H(m,l)$ onto the normalized PC in Eq. 1, a characteristic spatial pattern can be deduced:

$$S_i(l) = PC_i(m) \cdot H(m,l) \quad (2)$$

The constraining indices (CI_i) are just the projection of H onto S:

$$CI_i(m) = H(m,l) \cdot S_i(l) \quad (3)$$

Similarly, the observation CI is calculated by projecting observed H onto the same S. It is to be reminded that the basic principle of selecting the right predictor H on the right space $l \in L$ is that $H(l)$ should have a good correlation with ECSP (the predictand) and a clear physical meaning.

We show in the main text that the main modes of inter-model spread for future ECSP change are closely associated with the historical mean state of tropical Pacific precipitation simulations. As an application of the above-described framework, our variables to be constrained would be the PC_i of inter-model spread in ECSP projection, while the constraining variable is the present-day precipitation in the constraining areas (black boxes in Fig. 2).

Implementation of the emergent constraint procedure

Our practical implementation of the emergent constraint (EC) to narrow the range of the projected ECSP follows what described in Chen et al.[21]. We firstly establish a link between future climate change (P or its principal components PC_i, also noted as Y, generally represented as the ordinate in the graphic representation) and present-day climate (H or its elaborated indices CI_i, also noted as X, in the abscissa). It is based on the linear regression between Y and X obtained from climate models:

$$Y = \bar{Y} + k(X - \bar{X}) \quad (4)$$

where k is the regression coefficient, Y the first two normalized leading principal components (PC_1 and PC_2), and X the corresponding constraining indices (CI_1 and CI_2) defined in Eq. 3. $\bar{X}$ and $\bar{Y}$ are multi-model ensemble mean of PC and constraining indices.

We use the observations in the current climate (X_o) to constrain Y, so the uncertainty in the observations should be considered. Under the

Gaussian assumptions that relate the observations to current climate[43], the signal-to-noise ratio (*SNR*) in the observation is the ratio between the variance across models (σ_X^2) and observational datasets (σ_O^2): $SNR = \sigma_X^2/\sigma_O^2$. The regression coefficient is multiplied by $\frac{1}{1+SNR^{-1}}$ to be corrected. If *SNR* is much larger than 1 (SNR ≫ 1), the effect of correction can be neglected. *SNR* of CI_1 is 15.8, and that of CI_2 is 35.0 in this work. Hence, combining Eq. 4 and the *SNR* correction, the constrained expectation ($\bar{Y}_c$) and variance ($\sigma^2_{\bar{Y}_c}$) can be expressed as:

$$\bar{Y}_c = \bar{Y} + \frac{k}{1+SNR^{-1}}(X_o - \bar{X}) \tag{5}$$

$$\sigma^2_{\bar{Y}_c} = \left(1 - \frac{r^2}{1+SNR^{-1}}\right)\sigma^2_Y \tag{6}$$

where r denotes the correlation coefficient between X and Y, σ_Y denotes the standard deviation of Y across models.

Based on Eq. 6, the relative variance reduction $(1-\frac{\sigma^2_{\bar{Y}_c}}{\sigma^2_Y})$ from the framework is $\frac{r^2}{1+SNR^{-1}}$. Thus, the total reduced variance (*TRV*) after constraining the *PC* can be expressed as the weighting on the corresponding explained variances of *PC* (*PCV*) in percentage:

$$TRV = \sum_{i=1}^{I} r_i^2 PCV_i \tag{7}$$

where r_i denotes the corrected correlation coefficient between *PC* and *CI* for mode *i*, PCV_i denotes the corresponding explained variance of *PC* for mode *i*.

The corrected PC_O (PC_{1O} and PC_{2O}) is estimated by the emergent constraint using mean of the observational *CI*. Then the multi-model mean projection of ECSP can be corrected with the EOF reconstruction, following Eq. 1:

$$P(n) \cong \overline{P(n)} + \sum_{i=1}^{I}\{PC_{io} \times EOF_i(n)\} \tag{8}$$

where subscript '*O*' denotes optimal *PC* constrained by observational precipitation, $P(n)$ denotes the multi-model ensemble mean of East China summer precipitation changes.

In summary, we can give a general flowchart (Supplementary Fig. S15) of the emergent constraint technique for ECSP projection. We first apply the typical empirical orthogonal function analysis to the ECSP projection to identify the leading modes of the inter-model spread. Potential constraining variables are then regressed onto the normalized *PC* (Predictand) to identify key areas with high projection coefficients, and construct constraining indices (Predictor). When the relationship between the Predictor and the Predictand is established, the remaining of emergent constraint procedure consists of using observational Predictor to correct Predictand, and finally to correct the ECSP projection by EOF reconstruction. What calls for special attention is that the above procedure only raises a proposed constraint, which is an emergent relationship with strong statistical underpinnings. Only when the emergent relationship is also associated with a plausible mechanism, it becomes a confirmed constraint. But even a proposed constraint can be valuable if associated with likelihood statements[18]. From the perspective of methodology, our technical processes could be widely applied in other regions and fields. But it is necessary to identify suitable indices that could serve as their predictors. Robust and physically explainable statistical relations are also a challenge for them.

Data availability

CMIP6 model data are from the Earth System Grid Federation [https://esgf-node.llnl.gov/search/cmip6/]. Observational precipitation CMAP and GPCP are provided by the NOAA/OAR/ESRL, PSD, Boulder, CO, USA [https://climatedataguide.ucar.edu/climate-data/].

Code availability

All data processing codes are available if a request is sent to the corresponding authors.

Received: 28 July 2024; Accepted: 26 November 2024;
Published online: 04 December 2024

References

1. Ding, Y. & Chan, J. The East Asian summer monsoon: an overview. *Meteorol. Atmos. Phys.* **89**, 117–142 (2005).
2. Wu, Q. et al. Asian summer monsoon responses to the change of land-sea thermodynamic contrast in a warming climate: CMIP6 projections. *Adv. Clim. Change Res.* **13**, 205–217 (2022).
3. Moon, S. & Ha, K. Future changes in monsoon duration and precipitation using CMIP6. *npj. Clim. Atmos. Sci.* **3**, 45 (2020).
4. Son, J., Seo, K. & Wang, B. Dynamical control of the Tibetan Plateau on the East Asian summer monsoon. *Geophys. Res. Lett.* **46**, 7672–7679 (2019).
5. Hu, K. et al. Interdecadal variations in ENSO influences on Northwest Pacific-East Asian early summertime climate simulated in CMIP5 models. *J. Clim.* **27**, 5982–5998 (2014).
6. Ren, Y., Zhou, B., Song, L. & Xiao, Y. Interannual variability of western north Pacific subtropical high, East Asian jet and East Asian summer precipitation: CMIP5 simulation and projection. *Quat. Int.* **440**, 64–70 (2017).
7. Liu, Y., Li, Y. & Ding, Y. East Asian summer rainfall projection and uncertainty under a global warming scenario. *Int. J. Climatol.* **40**, 4828–4842 (2020).
8. Zou, L. & Zhou, T. Mean and extreme precipitation changes over China under SSP scenarios: Results from high resolution dynamical downscaling for CORDEX East Asia. *Clim. Dyn.* **58**, 1015–1031 (2020).
9. He, C., Wang, Z., Zhou, T. & Li, T. Enhanced latent heating over the Tibetan Plateau as a key to the enhanced East Asian summer monsoon circulation under a warming climate. *J. Clim.* **32**, 3373–3388 (2019).
10. Kitoh, A. et al. Monsoons in a changing world: a regional perspective in a global context. *J. Geophys. Res. Atmos.* **118**, 3053–3065 (2013).
11. Sooraj, K., Terray, P. & Mujumdar, M. Global warming and the weakening of the Asian summer monsoon circulation: Assessments from the CMIP5 models. *Clim. Dyn.* **45**, 233–252 (2015).
12. Zhou, S., Huang, P., Huang, G. & Hu, K. Leading source and constraint on the systematic spread of the changes in East Asian and western North Pacific summer monsoon. *Environ. Res. Lett.* **14**, 124059 (2019).
13. You, Q. et al. Recent frontiers of climate changes in East Asia at global warming of 1.5 °C and 2 °C. *npj Clim. Atmos. Sci.* **5**, 1–17 (2022).
14. Zhu, H., Jiang, Z. & Li, L. Projection of climate extremes in China, an incremental exercise from CMIP5 to CMIP6. *Sci. Bull.* **66**, 2528–2537 (2021).
15. Zhu, H. et al. Intercomparison of multi-model ensemble-processing strategies within a consistent framework for climate projection in China. *Sci. China Earth. Sci.* **66**, 2125–2141 (2023).
16. Wang, X., Jiang, D. & Lang, X. Temperature and precipitation changes over China under a 1.5°C global warming scenario based on CMIP5 Models (in Chinese). *Chin. J. Atmos. Sci.* **43**, 1158–1170 (2019).
17. Caldwell, P., Zelinka, M. & Klein, S. Evaluating emergent constraints on equilibrium climate sensitivity. *J. Clim.* **31**, 3921–3942 (2018).
18. Hall, A., Cox, P., Huntingford, C. & Klein, S. Progressing emergent constraints on future climate change. *Nat. Clim. Change* **9**, 269–278 (2019).
19. Brient, F. Reducing uncertainties in climate projections with emergent constraints: concepts, examples and prospects. *Adv. Atmos. Sci.* **37**, 1–15 (2020).
20. Wang, X. et al. Emergent constraint on crop yield response to warmer temperature from field experiments. *Nat. Sustain.* **3**, 908–916 (2020).

21. Chen, X., Zhou, T., Wu, P., Guo, Z. & Wang, M. Emergent constraints on future projections of the western North Pacific Subtropical High. *Nat. Commun.* **11**, 2802 (2020).
22. Chen, Z. et al. Observationally constrained projection of Afro-Asian monsoon precipitation. *Nat. Commun.* **13**, 2552 (2022).
23. Dong, Y. et al. Intermodel spread in the pattern effect and its contribution to climate sensitivity in CMIP5 and CMIP6 Models. *J. Clim.* **33**, 7755–7775 (2020).
24. Zhou, C. et al. Greater committed warming after accounting for the pattern effect. *Nat. Clim. Change* **11**, 132–136 (2021).
25. Armor, K. et al. Sea-surface temperature pattern effects have slowed global warming and biased warming-based constraints on climate sensitivity. *P. Natl Acad. Sci. Usa.* **121**, e2312093121 (2024).
26. Li, C., Li, X., Yang, H., Pan, J. & Li, G. Tropical Pacific-Indian Ocean associated mode and its climatic impacts (in Chinese). *Chin. J. Atmos. Sci.* **42**, 505–523 (2018).
27. Li, G., Xie, S., He, C. & Chen, Z. Western Pacifc emergent constraint lowers projected increase in Indian summer monsoon rainfall. *Nat. Clim. Change* **7**, 708–712 (2017).
28. Yang, Y., Park, J., An, S., Wang, B. & Xiao, L. Mean sea surface temperature changes influence ENSO-related precipitation changes in the mid-latitudes. *Nat. Commun.* **12**, 1495 (2021).
29. Wen, N., Li, L. & Hao, Y. Response of East Asian summer precipitation to intermediate SST anomalies while El Niño decays and dependence on type of events. *J. Clim.* **35**, 3845–3860 (2022).
30. Wang, B. et al. Understanding the recent increase in multiyear La Niñas. *Nat. Clim. Change* **13**, 1075–1081 (2023).
31. Dong, L., Leung, L., Lu, J. & Song, F. Double-ITCZ as an emergent constraint for future precipitation over Mediterranean climate regions in the North Hemisphere. *Geophys. Res. Lett.* **48**, e2020GL091569 (2021).
32. Zhou, S., Huang, G. & Huang, P. A bias-corrected projection for the changes in East Asian summer monsoon rainfall under global warming. *Clim. Dyn.* **54**, 1–16 (2020).
33. Shiogama, H., Watanabe, M., Kim, H. & Hirota, N. Emergent constraints on future precipitation changes. *Nature* **602**, 612–616 (2022).
34. Paik, S., An, S., Min, S., King, A. & Kim, S. Emergent constraints on future extreme precipitation intensification: from global to continental scales. *Weather. Clim. Extrem.* **42**, 100613 (2023).
35. Shiogama, H., Hayashi, M., Hirota, H. & Ogura, T. Emergent constraints on future changes in several climate variables and extreme indices from global to regional scales. *SOLA* **20**, 122–129 (2024).
36. Dai, P. et al. Constraints on regional projections of mean and extreme precipitation under warming. *P. Natl Acad. Sci. USA* **121**, e2312400121 (2024).
37. Nijsse, F., Cox, P., Huntingford, C. & Williamson, M. Decadal global temperature variability increases strongly with climate sensitivity. *Nat. Clim. Change* **9**, 598–601 (2019).
38. Williamson, M. et al. Emergent constraints on climate sensitivities. *Rev. Mod. Phys.* **93**, 025004 (2021).
39. Rowell, D. An observational constraint on CMIP5 projections of the East African long rains and Southern Indian Ocean warming. *Geophys. Res. Lett.* **46**, 6050–6058 (2019).
40. O'Neill, B. et al. The scenario model intercomparison project (ScenarioMIP) for CMIP6. *Geosci. Model. Dev.* **9**, 3461–3482 (2016).
41. Adler, R. et al. The version-2 global precipitation climatology project (GPCP) monthly precipitation analysis (1979-present). *J. Hydrometeorol.* **4**, 1147–1167 (2003).
42. Xie, P. & Arkin, P. Global precipitation: a 17-year monthly analysis based on gauge observations, satellite estimates, and numerical model outputs. *Bull. Am. Meteorol. Soc.* **78**, 2539–2558 (1997).
43. Bowman, K., Cressie, N., Qu, X. & Hall, A. A hierarchical statistical framework for emergent constraints: application to snow-albedo feedback. *Geophys. Res. Lett.* **45**, 13050–13059 (2018).

Acknowledgements

We would like to acknowledge the World Climate Research Program's Working Group on Coupled Modeling, which is responsible for CMIP6. We thank the climate modeling groups for producing simulations and making their model outputs available. This work was supported by the National Natural Science Foundation of China (42275184 and 42430609), the Natural Science Foundation of Jiangsu Province (BK20240317), the Wuxi University Research Start-up Fund for Introduced Talents (2024r041), and the Joint Open Project of Key Laboratory of Meteorological Disaster, Ministry of Education & Collaborative Innovation Center on Forecast and Evaluation of Meteorological Disasters, NUIST (KLME202405).

Author contributions

H.H.Z. designed the research, performed the analysis, drafted and revised the manuscript. Z.H.J. conceiverd the idea and designed the study, provided comments, and revised the manuscript. L.L. supervised the work, provided comments, and revised the manuscript. W. L. and S. J. performed the analysis and revised the manuscript. All co-authors contributed to the paper and approved the submitted version.

Competing interests

The authors declare no competing interests.

Additional information

Supplementary information The online version contains supplementary material available at https://doi.org/10.1038/s41612-024-00863-3.

Correspondence and requests for materials should be addressed to Zhihong Jiang.